BioMedical Engineering OnLine

Research

Evaluation of a fiberoptic-based system for measurement of optical properties in highly attenuating turbid media

Divyesh Sharma, Anant Agrawal, L Stephanie Matchette and T Joshua Pfefer*

Address: Food and Drug Administration, Center for Devices and Radiological Health, Rockville, Maryland, USA

Email: Divyesh Sharma - divyesh_sharma2001@yahoo.com; Anant Agrawal - anant.agrawal@fda.hhs.gov; L
Stephanie Matchette - stephanie.matchette@fda.hhs.gov; T Joshua Pfefer* - joshua.pfefer@fda.hhs.gov

* Corresponding author

Abstract

Background: Accurate measurements of the optical properties of biological tissue in the ultraviolet A and short visible wavelengths are needed to achieve a quantitative understanding of novel optical diagnostic devices. Currently, there is minimal information on optical property measurement approaches that are appropriate for *in vivo* measurements in highly absorbing and scattering tissues. We describe a novel fiberoptic-based reflectance system for measurement of optical properties in highly attenuating turbid media and provide an extensive *in vitro* evaluation of its accuracy. The influence of collecting reflectance at the illumination fiber on estimation accuracy is also investigated.

Methods: A neural network algorithm and reflectance distributions from Monte Carlo simulations were used to generate predictive models based on the two geometries. Absolute measurements of diffuse reflectance were enabled through calibration of the reflectance system. Spatially-resolved reflectance distributions were measured in tissue phantoms at 405 nm for absorption coefficients (μ_a) from 1 to 25 cm^{-1} and reduced scattering coefficients (μ_s') from 5 to 25 cm^{-1}. These data and predictive models were used to estimate the optical properties of tissue-simulating phantoms.

Results: By comparing predicted and known optical properties, the average errors for μ_a and μ_s' were found to be 3.0% and 4.6%, respectively, for a linear probe approach. When bifurcated probe data was included and samples with μ_a values less than 5 cm^{-1} were excluded, predictive errors for μ_a and μ_s' were further reduced to 1.8% and 3.5%.

Conclusion: Improvements in system design have led to significant reductions in optical property estimation error. While the incorporation of a bifurcated illumination fiber shows promise for improving the accuracy of μ_s' estimates, further study of this approach is needed to elucidate the source of discrepancies between measurements and simulation results at low μ_a values.

Background

In recent years, advances in optical technology have helped facilitate rapid progress in fluorescence and reflectance spectroscopy-based techniques for medical diagnostics. Recent studies involving ultraviolet A (UVA, 320 to 400 nm) and shorter visible (VIS) wavelengths (400 to 550 nm) have demonstrated that spectroscopic approaches can be highly effective for a variety of applications including intravascular detection of atherosclerotic plaque [1], *in situ* brain tumor demarcation [2] and surveillance for neoplasia in mucosal tissues that line organs such as the lungs and cervix [3]. While clinical studies

have shown significant promise, further improvements in efficacy are needed for this technology to achieve its full potential.

Accurate approaches for *in vivo* measurement of tissue optical properties in UVA and short VIS wavelengths are needed to optimize the ability of diagnostic devices. Since some tissue discrimination algorithms [4] use optical property data as inputs, the accuracy of this data may directly influence a system's diagnostic efficacy. Furthermore, numerical and analytical models are effective tools for elucidating light-tissue interaction phenomena and identifying optimal device designs, including selection of excitation and collection wavelengths and probe geometry [5,6]. However, the accuracy of input parameters such as tissue optical properties can strongly influence the quality and usefulness of modeling results.

The most important optical properties for describing light propagation in tissue are absorption coefficient (μ_a) and reduced scattering coefficient $\{ \mu_s' = \mu_s(1\text{-}g) \}$, which is a convenient combination of the scattering coefficient (μ_s) and the scattering phase function (g). While prior optical property studies have typically involved VIS to near-infrared wavelengths where tissue tends to have relatively low attenuation levels [7], data on *in vivo* optical properties in the UVA and lower VIS wavelength ranges are limited. This is likely due in part to the fact that many earlier studies were performed in support of photon migration applications. Another factor may have been the difficulties associated with measuring signals in tissue with high attenuation levels, such as the rapid decay in reflected light levels with distance from the source location.

In spite of the limited literature on optical property measurements at relevant UVA and short VIS wavelengths, prior studies at longer wavelengths have produced significant advances in experimental, computational and analytical techniques, some of which are applicable in our spectral range of interest. While time-[8] and frequency-[9] domain approaches have shown promise at long VIS and near-infrared wavelengths, these approaches tend to be expensive and have not shown efficacy at shorter wavelengths. Spatially-resolved approaches typically involve using tissue phantoms or computer simulations to generate data for inverse model calibration, and then using the model to estimate optical properties based on reflectance measurements [10]. In prior studies, diffuse reflectance has been collected from tissue phantoms over a broad range of optical properties and wavelengths [10-12]. Monte Carlo [10,11] or diffusion approximation [13] light propagation models are typically used to generate spatially-resolved reflectance profiles, although the latter

are limited to larger source-detector separation distances which satisfy diffusion criteria. Reflectance measurements are typically performed with multiple-channel fiberoptic bundles, or probes, which deliver light to the tissue surface and collect reflectance at two or more well-defined distances from the source fiber. Optical fibers are commonly arranged in either circular [11-14] or linear [15,16] patterns on the face of the fiberoptic probe. The source-collection separation distances used in prior studies have ranged from several millimeters to centimeters [11,14-18]. Properties such as numerical aperture (NA) and fiber diameter have varied widely in prior studies. One recent study involved an approach based on bifurcated probes of varying aperture diameter, rather than the more typical linear array approach [19]. Multivariate calibration techniques such as neural networks (NN) [10,13,20], fuzzy logic [21], regression [11] and partial least squares [22] have been used to solve the inverse problem of determining optical properties from reflectance.

In a prior pilot study, we evaluated several different approaches to fiberoptic probe-based optical property determination using Monte Carlo simulations and diffuse reflectance measurements [23]. By calibrating a neural network model with simulated reflectance data based on uniformly distributed optical properties and validating the model with measurements of tissue phantoms having randomly distributed optical properties, moderately high levels of accuracy were found: root mean square errors of 1.58 cm^{-1} for μ_a and 2.35 cm^{-1} for μ_s'. These values translate to average predictive errors of 12.5% and 16.2%. Optical property estimation errors may be attributed in part to the measurement approach in which large variations in intensity from fiber-to-fiber were produced at the CCD camera, as well as the limited dynamic range (14-bit) and noise levels generated during long exposures. In general, these results were sufficient for a pilot study, yet they indicated that refinements would be needed before accurate *in vivo* measurements could be achieved.

In an effort to improve upon the results of the pilot study and develop a system that is sufficiently accurate to provide meaningful data during *in vivo* measurements, significant modifications were made to the prior system. The goals of the current study were to evaluate the accuracy of this second generation optical property measurement system and assess the potential added benefit of a bifurcated fiberoptic probe that enables detection of reflectance from the illumination site.
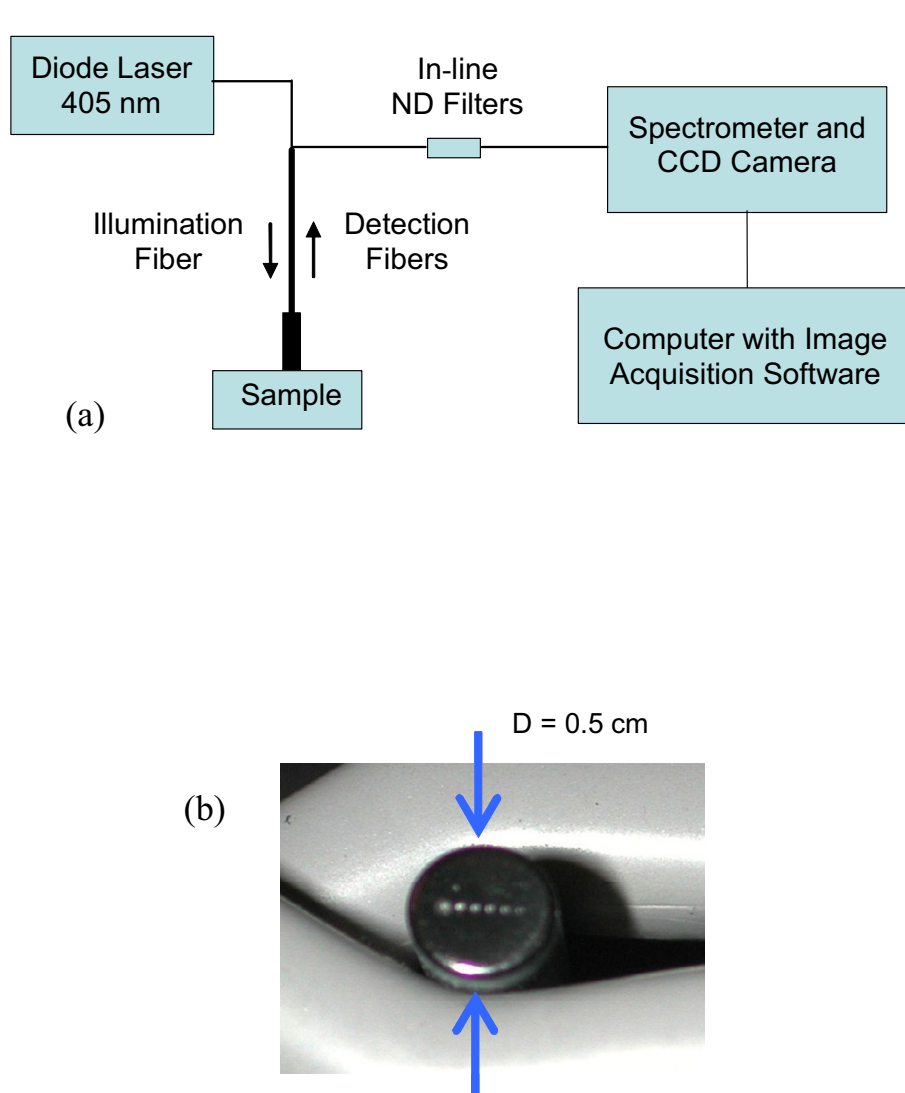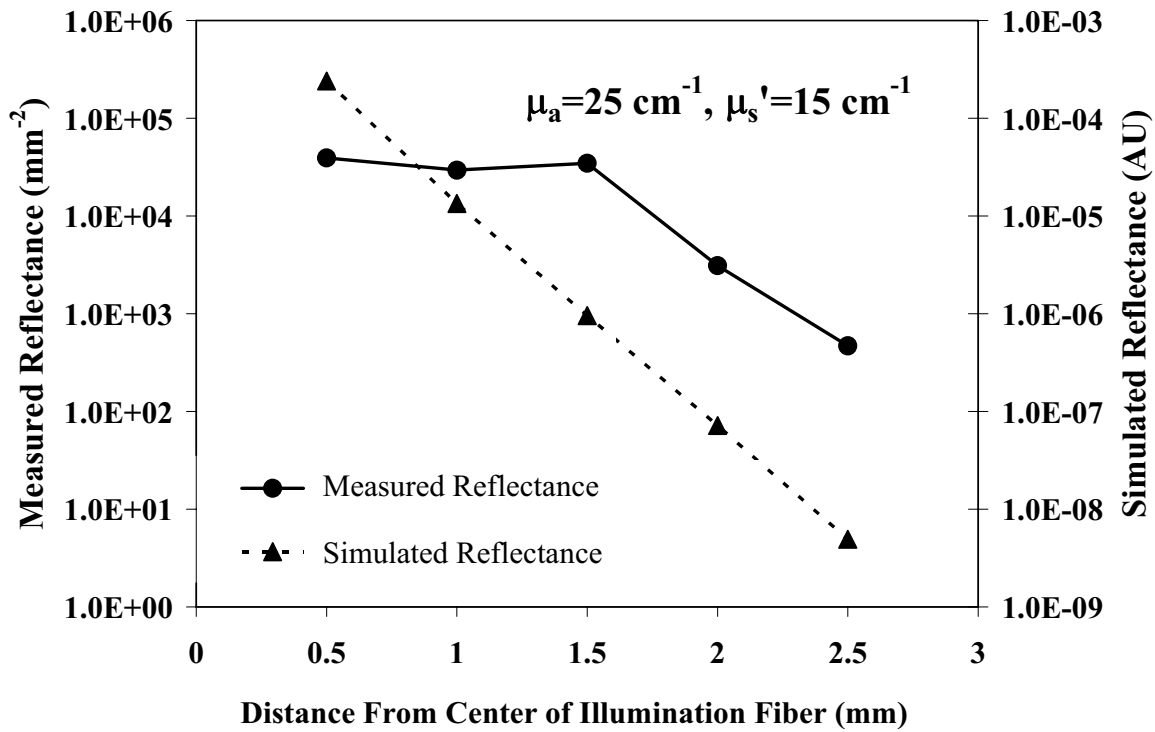
Figure 1
System Diagram. Diagram includes (a) experimental setup and (b) fiberoptic probe face.

Methods

System description

Diagrams of the experimental setup and fiberoptic probe face used to perform diffuse reflectance measurements are presented in Figure 1. The source is a 405 nm diode laser (LCDU 12/5431, Power Technology, Inc; Little Rock, AR) with a power level of 2.5 mW. The input power is adjusted using neutral density (ND) filters (CVI Laser Corporation, Albuquerque, NM). The custom designed fiberoptic probe (FiberTech Optica, Ontario, Canada) is used to deliver laser light from the source to the sample and guide diffuse reflectance from the sample to the detector. The diameter of the probe face is 0.5 cm which would make it practical for *in vivo* studies of internal organ sites. The probe con-tains a single illumination fiber and five detection fibers spaced at consecutive center-to-center distances of 0.5 mm. The core diameter of each fiber is 0.2 mm with a NA of 0.22. The detection legs are connected to five in-line fil-ters (FHS-UV, Ocean Optics, Dunedin, FL) three of which contained ND filters. The filter holders are coupled to the legs of a second probe, the common end of which con-tains a linear fiber array that was aligned to the entrance slit of an imaging spectrometer (SpectraPro 300i, Acton Research Corp., Acton, MA). The output of the spectrom-eter is detected by a low noise, high dynamic range (16-bit) CCD camera (Princeton Instruments Spec10:400B, Trenton, New Jersey) and acquired using proprietary soft-ware (WinSpec Princeton Instruments, Trenton, NJ).
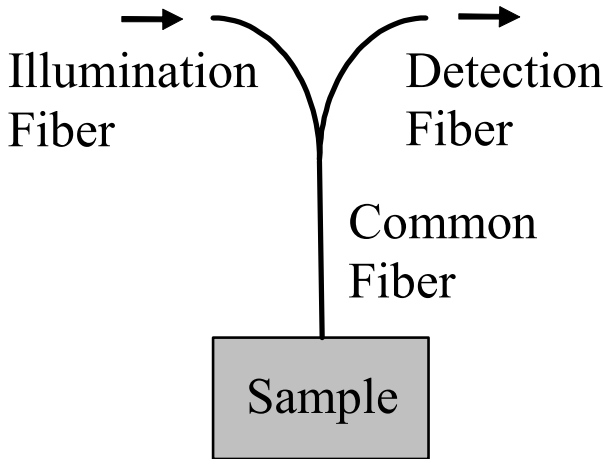
Figure 2

Reduction of detected signal range. Monte Carlo simulations and experimental data for μ_a = 25 cm^{-1}, μ_s' = 15 cm^{-1}. The signal range in the experimental data was reduced by using neutral density filters to preferentially attenuate the channels closest to the source fiber.

Experimental system modifications

In our previous system, the large range of light levels (Figure 2) incident on the detector necessitated measurements at multiple exposure durations to acquire a single reflectance distribution. By improving the homogeneity of light levels delivered by the fiberoptic probe, a single CCD acquisition could record all fiber intensities. This was achieved by using in-line ND filters [24] for each fiber. By analyzing the detected signal levels for four samples at the edges of the designated optical property parameter space (μ_a = 1, 25 cm^{-1}, μ_s' = 5, 25 cm^{-1}) we identified a combination of ND filters for each fiber which would produce moderately high output levels on the CCD without inducing saturation. Combined attenuation levels of 2.2, 1.9, and 0.3 OD were used for the fibers at separation distances of 0.5, 1.0 and 2.0 mm. The ND levels chosen for these fibers appear irregular due to variations in fiber transmittance and in coupling efficiency of the in-line filters. Thus the system was optimized in such a way that a single set of ND filters could be used to collect reflectance for *in vitro* or *in vivo* samples having optical properties

anywhere within the relevant range (μ_a = 1–25 cm^{-1}, μ_s' = 5–25 cm^{-1}). Figure 2 shows computational modeling results for a sample with μ_a = 25 cm^{-1}, μ_s' = 15 cm^{-1} in order to illustrate the wide range of intensities that must be detected. This graph also includes a measurement of a tissue phantom with the same optical properties, indicating that the variation of intensity at the CCD has been reduced from five orders of magnitude to two through the use of ND filters. The exposure duration required for acquiring sufficient signal ranged from 0.12 to 25 seconds depending on the sample attenuation level.

The second optimization task involved enabling absolute measurements by calibrating the measured intensity to simulation results. In order to accomplish this goal, CCD measurements for all detection fibers were made at two different illumination intensities in three different phantoms : μ_a = 1 cm^{-1} and μ_s' = 5 cm^{-1}, μ_a = 1 cm^{-1} and μ_s' = 25 cm^{-1} and μ_a = 2 cm^{-1} and μ_s' = 25 cm^{-1}. For each fiber position, the relationship between measured CCD counts and Monte Carlo-predicted intensity levels were graphed

Figure 3
Diagram of bifurcated probe. A bifurcated fiberoptic probe was used to measure reflectance at the illumination site.

for the two phantoms. A linear fit to these points and the origin was calculated for each fiber. These linear fits were used as calibration equations to convert CCD counts to absolute intensity levels for all measurements during this study.

Bifurcated fiberoptic probe measurements
The objective of this component of the study was to evaluate the utility of adding a bifurcated illumination fiber to the linear-array geometry. This work was performed for two primary reasons: (1) computational results that indicate that at positions near the illumination fiber there is a relatively high level of variation in reflectance intensity as μ_s' changes [23]; and (2) a prior investigation has indicated that a sized-fiber approach involving collecting reflectance at the site of illumination is highly effective for determining tissue optical properties [19]. A bifurcated fiberoptic probe (Innova Quartz, Phoenix, AZ) – illumination and collection fibers fused to a third common fiber which contacted the sample – with a core diameter of 0.2 mm and NA of 0.22 was used to perform the measurements (Figure 3) [25]. Light collected from the detection leg of the probe was measured by a power meter (Newport Model 1930C, 818-ST-UV detector, Irvine, CA) for each of the 60 samples previously used for the linear array measurements.

The reflectance collected at the illumination site of the sample is the total reflectance (R_{total}) which consists of

two components: diffuse reflectance ($R_{diffuse}$) and specular reflectance ($R_{specular}$). Fresnel reflections for both fiber core/air and fiber core/water were measured. The probe geometry resulted in multiple reflections at the bifurcation point. Thus, baseline reflectance measurement was made using fiber core refractive index matching liquid (n = 1.47, Cargille Laboratories, Inc; Cedar Grove, NJ). $R_{diffuse}$ was obtained by normalizing all the data points to the Fresnel reflections for the fiber core/water as shown below:

$$R_{diffuse} = R_{total} - R_{specular} \quad (1)$$

$$R_{total} = \frac{\left(P_{sample} - P_\eta \right)}{E.F. * P_{input}} \quad (2)$$

$$R_{specular} = \frac{\left(P_{water} - P_\eta \right)}{E.F. * P_{input}} \quad (3)$$

Where,

P_{sample} = Power measured from the sample

P_η = Power measured from the index matching liquid

P_{water} = Power output from fiber core/water

P_{input} = Power output from the probe

$E.F.$ = Fiber efficiency factor obtained for the collection fiber

Experimentally measured Fresnel reflectance was within 10% of the theoretical value for the fiber core/water interface. The fiber efficiency factor was obtained by coupling light from a 100 μm core diameter fiber into the common end of the bifurcated fiber and measuring the output from the detection leg of the probe. Measurements were made on the same sets of phantoms used for linear-array fiber system.

Tissue phantoms
Since the validity of the system evaluation is dependent on the accuracy of tissue phantom optical properties, evaluation of phantom materials and benchmarking of phantoms was performed at the outset of this study. The optical properties of individual tissue phantoms were determined using an inverse adding-doubling approach [26] and a spectrophotometer (Shimadzu UV-3101PC, Columbia, MD). This data was compared to theoretical estimates based on Mie theory and direct collimated absorption measurements of the scatterer and absorber, respectively.

Polystyrene microspheres have been used to provide scattering for tissue phantoms in prior studies due to their minimal levels of fluorescence and absorbance as well as their ability to remain in suspension for a long durations. Furthermore, microspheres have a g value which is close to that of biological tissue [27,28]. In order to achieve a g of approximately 0.9, microspheres with a particle size of 1.053 µm (and thus a g of 0.912) were chosen for this study. In order to insure that the absorber used was a pure absorber, absorption and thus transmission should be linear with the concentration in the desired range of absorption coefficient. These measurements were validated against an independent laser setup. As observed in a prior study [29], India ink is particulate in nature with a significant scattering component. Thus, Nigrosin which is the most common absorber cited in literature and which has a linear transmittance with concentration, was chosen as the absorber. The stock absorption coefficient was measured in a spectrophotometer and subsequently diluted to get the required μ_a for the phantom within the range 1 to 25 cm^{-1}.

For the reflectance study, a set of 10 phantoms with uniform optical properties and a set of 60 phantoms with random optical properties were constructed. All phantoms were in liquid form, which enabled us to slightly submerge the tip of the fiberoptic probe for optimal fiber-sample coupling. The uniform optical properties had the following values: 1) with μ_a held constant at 15 cm^{-1} and μ_s' = 5, 10, 15, 20 and 25 cm^{-1}; and, 2) with μ_s' held constant at 15 cm^{-1} and μ_a = 1, 5, 10, 15, 20 and 25 cm^{-1}. The random optical properties were distributed over a μ_a range of 1 to 25 cm^{-1} and μ_s' range of 5 to 25 cm^{-1}.

Neural network modeling

Evaluation of the optical property measurement technique was performed by developing a NN based inverse model [23] which when provided reflectance data collected from a sample will generate an estimation of μ_a and μ_s'. The NN algorithm implemented a feed-forward back-propagation network with a Levenburg-Marquardt training function. The input layer contained five and six nodes for the linear array and bifurcated designs, respectively. The output layer contained two nodes, for the predicted optical properties. Optical property calculations were performed offline and required minimal processing time (< 1 sec) for data files that incorporated as many as 60 samples.

Raw reflectance data from computational or experimental results for linear-array probe were preprocessed prior to use in the neural network model:

$$S = -\log R \quad (4)$$

where R is the power of the detected reflectance normalized to the illumination power. NN model calibration was performed using 30 sets of simulated-uniform reflectance (S) distributions, generated by the Monte Carlo modeling approach described previously [23,30]. Validation was performed against the 30 simulated-uniform (self-validation) and 60 measured phantoms with randomly distributed optical properties.

The linear-array probe data used to calibrate and test the NN models contained reflectance sets comprised of five S values, corresponding to the five detection fibers. When evaluating the models for the bifurcated probe system, the sixth unprocessed (no log taken) reflectance value – $R_{diffuse}$ from the illumination site – was added to the linear-array data.

The NN prediction results were analyzed according to the percent deviation from the expected values as follows:

$$\%Error = \frac{\left(\mu_{True} - \mu_{Estimated} \right)}{\mu_{True}} \quad (5)$$

$$\overline{\%Error} = \frac{\sum_{i=1}^{i=n} \left| Error_i \right|}{n} \quad (6)$$

Equation (5) denotes the formula used to generate each of the error data points in the results graphs, whereas equation (6) was used to calculate the overall error for a set of data.

Results
Validation of calibrated system

Initial validation of the fiberoptic based diffuse reflectance was carried out for the linear-array probe system. The calibration curves for converting CCD pixel counts to absolute intensity measurements were well-behaved, producing linear fits with R^2 values of 0.99 for all five detection fibers. Comparisons between experimental phantom measurements and Monte Carlo simulations for uniformly distributed optical property pairs (n = 10) indicated excellent agreement over a wide range of μ_a and μ_s' values (Figure 4).
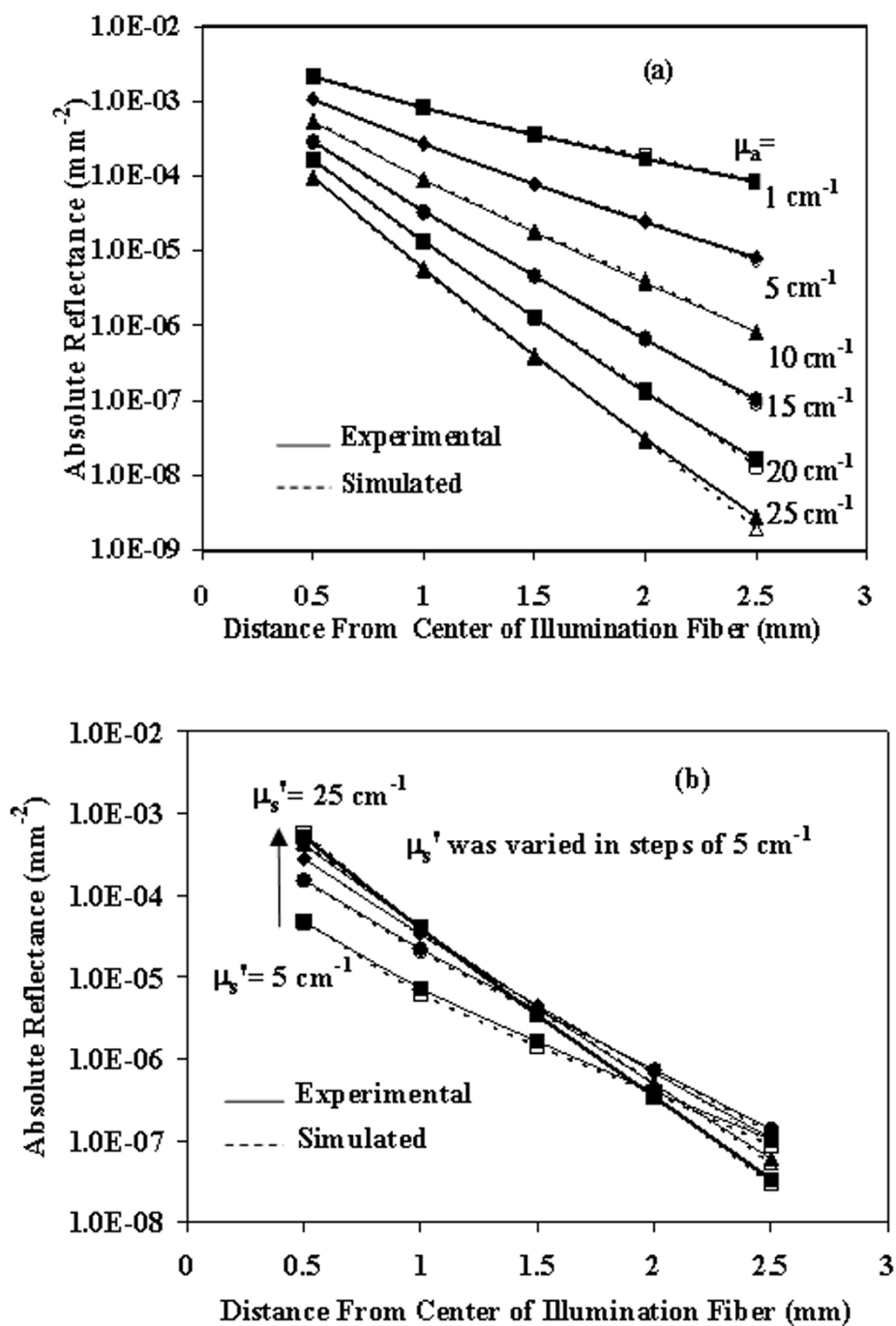
Figure 4
Comparison of experimental and simulated reflectance with linear array probe. These graphs present absolute diffuse reflectance data as determined by experimental measurements (filled shapes) and Monte Carlo simulations (open shapes). Graph (a) shows the effect of μ_a on reflectance when μ_s' is held constant at 15 cm^{-1}, whereas (b) shows the effect of μ_s on the reflectance when μ_a is held constant at 15 cm^{-1}.

Table 1: Evaluation of predictive NN models for the linear-array probe system.

	$E_{simulated}$ (n = 30)	$E_{measured}$ (n = 60)
Case A: All Samples		
μ_a	1.6%	3.2%
μ_s'	0.9%	5.6%
Case B: Samples with $\mu_a > 5$ cm^{-1}		
μ_a	1.0%	2.2%
μ_s'	1.0%	4.6%

Average errors (E) in prediction of absorption and reduced scattering coefficients are presented for two types of data sets: simulated (uniformly-distributed optical properties) and measured (randomly-distributed optical properties). Case A includes evaluation for the entire optical property range whereas for Case B, samples with $\mu_a < 5$ cm^{-1} are omitted.

Linear-array probe

A self-validation analysis was performed on simulated data to evaluate the performance and the theoretical limit of inverse model accuracy. The results of this analysis are shown in terms of mean prediction error in Table 1. Experimental evaluation was performed by measuring reflectance in 60 tissue phantoms with random optical properties over the following ranges: μ_a from 1 to 25 cm^{-1} and μ_s' from 5 to 25 cm^{-1}. The optical property prediction accuracy for each measurement is displayed in Figure 5, with mean values displayed in Table 1. Low levels of error – less than 6% – are seen across most of the μ_a range (3 cm^{-1} up to 25 cm^{-1}). However, in the $\mu_a < 3$ cm^{-1} region, accuracy degraded rapidly, with four data points showing errors of 14–19%. This increased error is likely due to two factors: (a) the accuracy of the neural network routine degrades at the boundaries of the range over which it was calibrated and (b) since the μ_a values in the aforementioned region are small, the same absolute levels of error

Table 2: Evaluation of predictive NN models for the combined linear-array/bifurcated probe approach.

	$E_{simulated}$ (n = 30)	$E_{measured}$ (n = 60)
Case A: All samples		
μ_a	2.1%	4.0%
μ_s'	0.7%	5.5%
Case B: Samples with $\mu_a > 5$ cm^{-1}		
μ_a	0.9%	2.2%
μ_s'	0.7%	3.7%

The cases and data sets in this table are the same as for Table 1.

that occur for larger μ_a values result in much greater percentage errors. Figure 5b indicates that although the vast majority of μ_s' predictions were within ± 10% of the true value, a minor trend towards under-prediction at higher μ_s' values is seen. Two of the 20% under-predictions in this graph occurred for samples in which the true μ_a value was low and prediction error for μ_a was large. The data point showing the greatest error in μ_s' (43%), however, did not occur for a sample in which μ_a error was high. One potential reason for this error may be air bubbles at the fiber tip which disrupt the fiber-sample coupling.

A summary of mean errors is presented in Table 1 for both the self-validation and experimental evaluation data. While the self-validation data set shows less error for μ_s' than for μ_a, measured results indicate the opposite trend. The reason for this is addressed in the discussion section. In general, the self-validation results indicate significantly better estimations than the experimental results, due in part to unavoidable experimental errors (e.g., noise in the detected signal, nonuniformity of the sample, imperfect coupling, etc.). These small errors tend to be amplified for small μ_a values, due to the two factors mentioned in the prior paragraph. Nevertheless, over the vast majority of the optical property range of interest, our approach provides a mean error level of less than 5%.

Bifurcated probe and combined approach

Initial measurements were performed to assess the accuracy of bifurcated probe technique. A comparison of measured reflectance and simulated data for a range of μ_a and μ_s' values is presented in Figure 6. Excellent agreement is observed between experimental and simulated data for most cases. However, a small deviation is seen at $\mu_a = 5$ cm^{-1} and a large (25%) deviation is seen for $\mu_a = 1$ cm^{-1}.

A predictive model was calibrated using simulated reflectance data corresponding to both linear array and bifurcated probe geometries. Self-validation analysis was performed using simulated data to evaluate the operation and theoretical limits of the model. The mean prediction errors for this case are presented in Table 2. The 60 tissue phantoms described in the prior section were then measured with the bifurcated probe and this data combined with the corresponding linear-array probe data. Prediction errors for this case are presented in Figure 7. The error
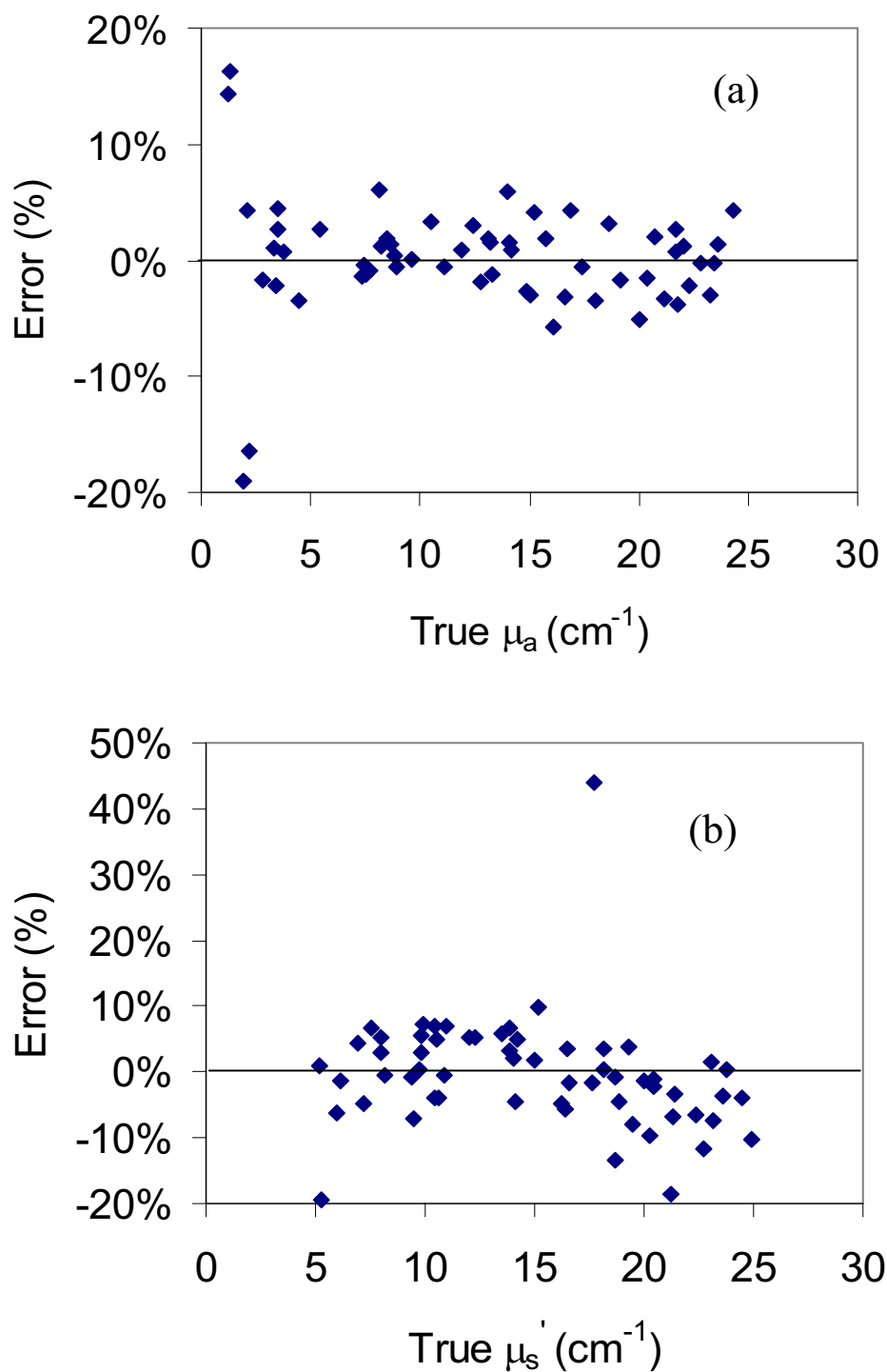
Figure 5
Accuracy of optical property estimates with linear array probe. These graphs present results for estimates of (a) μ_a and (b) μ_s'. Each of the 60 points represents the difference between predicted and true values.
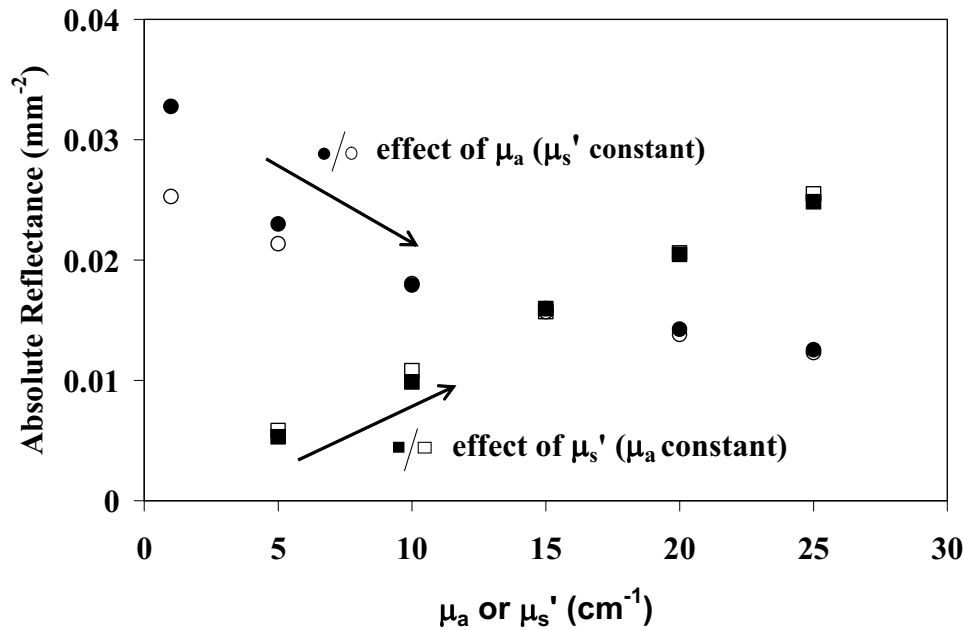
Figure 6
Accuracy of diffuse reflectance measurements with bifurcated probe. This graph provides a comparison of simulated (open shapes) and measured (filled shapes) diffuse reflectance for the bifurcated probe. Squares represent the effect of variations in μ'_s (for a constant μ_a = 15 cm^{-1}). Circles represent the effect of μ_a (for a constant μ'_s = 15 cm^{-1}).

graph for μ_a shows all five samples with true values of 2.2 cm^{-1} or less as being predicted with absolute errors of 14 to 42%. The model's difficulty with low μ_a samples also extended to μ'_s predictions, likely for the same reasons that large errors were produced at low optical property values for the linear array probe. Of the four data points showing the greatest μ'_s error levels, three corresponded to samples with μ_a values under 2.2 cm^{-1} that were poorly predicted by the model. The remaining value may be due to air bubbles as mentioned previously. Average percent errors (Table 2) for μ_a and μ'_s were calculated for simulated as well as experimental data using both the complete set of samples and a set containing only samples with μ_a values greater than 5 cm^{-1}. When the entire data set was considered, the addition of the bifurcated probe data caused an increase in error for μ_a while the μ'_s error level did not change appreciably. However, when the limited data set was analyzed, the change in geometry resulted in a 1% reduction in prediction error for μ'_s (a relative improvement of 24%) while the error for μ_a remained unchanged.

Discussion
Evaluation of reflectance measurements
Initial comparisons between measured and simulated data helped to validate the basic system performance for the linear array (Figure 4) and bifurcated fiber (Figure 6) probes. These graphs indicate that good agreement was achieved between the experimentally measured diffuse reflectance and simulation results over the entire range of optical properties studied. For the linear array probe, experimental and modeled data showed small discrepancies at the most distant fiber and highest μ_a values, as well as at lower μ'_s values. Bifurcated probe data show good agreement as well, with the exception of very low μ_a values, where the experimental values are significantly larger than the simulation data. Further discussion of the source of this discrepancy is provided in the "Analysis of Combined Probe Approach" section.

Notable trends in reflectance
Data in Figures 4 and 6 provide insight into general trends in reflectance as well as the performance of optical property estimation models. As seen in these figures and noted in our prior study [23], an increase in μ_a causes relatively
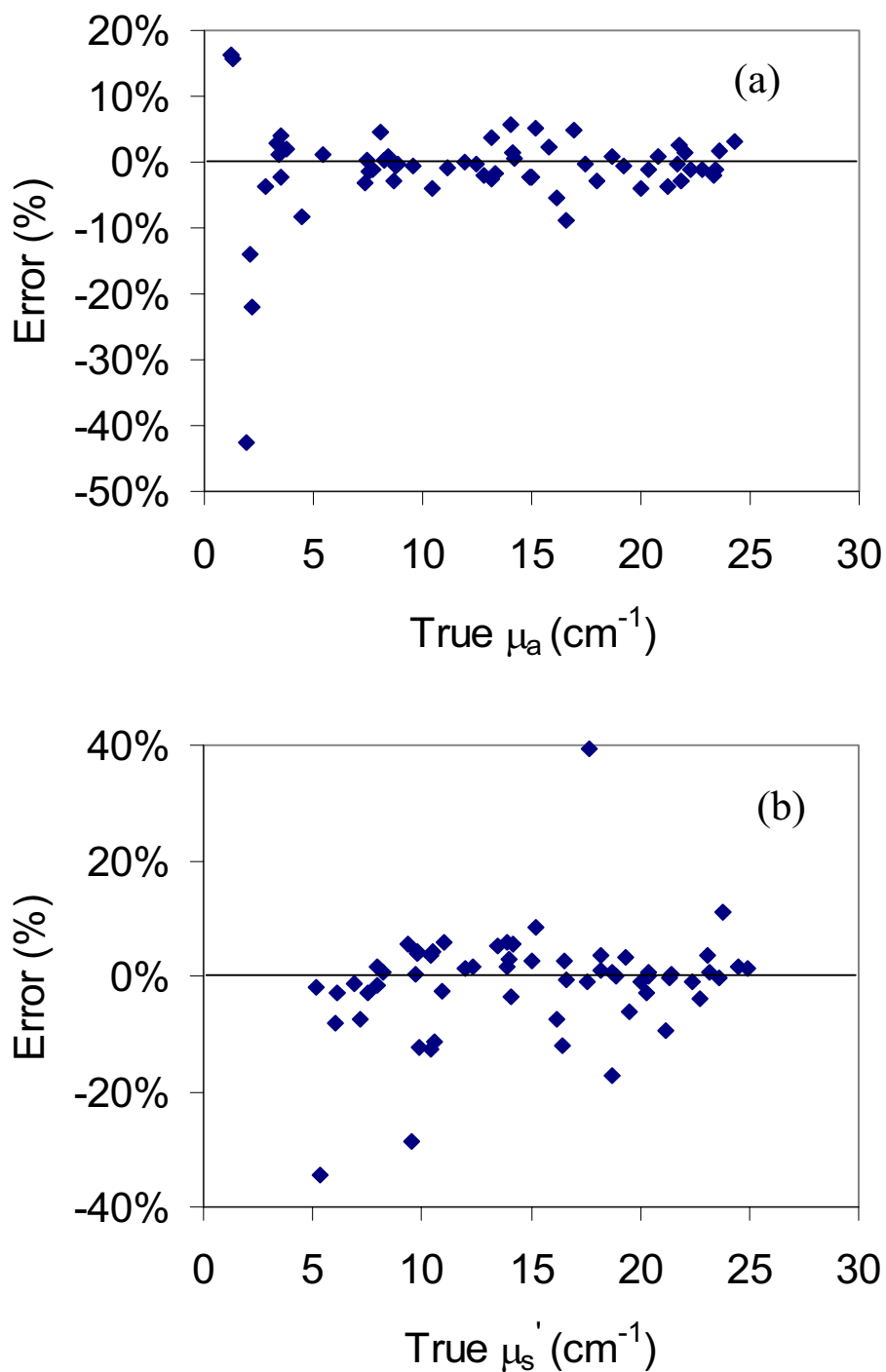
Figure 7
Accuracy of optical property estimates with combined linear-bifurcated probe. These graphs present results for estimates of (a) μ_a and (b) μ_s'. Each of the 60 data points represents the difference between predicted and true optical property values.

large decreases in reflectance, whereas increasing μ_s' produces less substantial variations. This is due to the fact that μ_a directly affects absorption of photons all along the path from source to detector, whereas μ_s', influences the diffuse nature of photon propagation which has a less direct influence on attenuation. Given the larger changes in reflectance with μ_a than μ_s', one would expect that for measurements with any significant level of error, the optical property estimation error would be greater for μ_s' than for μ_a. This was shown to be true for evaluations with experimental data (Tables 1 and 2). While the self-validation results produced equivalent or greater errors for μ_a than μ_s', these error levels were minimal. Figure 4a also indicates that the measured reflectance is slightly greater than the simulated reflectance for high μ_s' at the 2.5 mm position. These discrepancies appear to have been small enough to not significantly impact the predictions in Figure 5.

Reflectance data in Figure 4(b) indicate other interesting trends. Changes in reflectance intensity with μ_s' at the 0.5 mm fiber are significant when μ_s' values are small, but minimal when μ_s' is large. Conversely, at the 2.5 mm fiber, the change in reflectance as a function of μ_s' is small when μ_s' is low, and becomes larger at higher μ_s' values. Therefore, it is likely that reflectance from the 0.5 mm fiber is not very useful when μ_s' is high and reflectance from the 2.5 mm fiber is not very useful when μ_s' is low. Additionally, since reflectance at the 1.5 mm and 2 mm fibers does not appear to change significantly with μ_s', these values have minimal predictive value.

For the bifurcated probe geometry (Figure 6), increases in μ_s' produced an approximately linear increase in reflectance. As μ_s' was increased across the entire range from 5 to 25 cm⁻¹, reflectance increased by 370% This early result formed the basis of our hypothesis that reflectance data at the point of illumination might provide useful information on μ_s' which could be measured via a combined bifurcated-linear probe geometry.

Analysis of linear-array approach
The goal of this study was to develop a well-characterized second generation system that was highly accurate in the optical property range of interest. As mentioned previously, our prior system [23] was capable of estimating μ_a and μ_s' with average errors of 12.5% and 16.2%, respectively. In the current study, the best results for the full optical property range was provided by the linear-array approach, which enabled prediction of μ_a and μ_s' with errors of 3.2% and 5.6%, respectively. This represents reductions in error of 74% and 65% over our prior system. However, if the optical property range is restricted to include only μ_a values above 5 cm⁻¹, the combined approach provides even lower error levels: 2.2% and 3.7% for μ_a and μ_s', respectively. These results represent a significant improvement over our prior system and provide evidence that the current approach has strong potential to provide accurate estimates of *in vivo* optical properties.

Exact comparisons of current results with prior studies are not possible due to a lack of data for diffuse-reflectance based systems in the optical property range of interest. However, our findings compare favorably with the limited data available in the literature. In one recent study [31], tissue phantoms with μ_a values in the range of 1.3 cm⁻¹ to 31.8 cm⁻¹ were measured. The prediction error in this study ranged from 0.3% for a μ_a of 14.4 cm⁻¹ to 14% for a μ_a of 21.2 cm⁻¹. A second study [32] found accuracy levels within 10% for μ_a and 5% for μ_s' using tissue phantoms over an optical property range that included μ_a values from 0.6 to 3.3 cm⁻¹ and μ_s' values from 10 to 22 cm⁻¹. Not only are our current results comparable to those from prior studies in terms of prediction error, but the measurement of 60 random tissue phantoms enabled a more rigorous evaluation process than provided by prior studies.

Analysis of combined probe approach
The linear-array geometry (Table 1) produced a higher level of prediction accuracy for μ_a than for μ_s'. Given the initial results from bifurcated probe measurements (Figure 6), it was expected that the combined linear-bifurcated approach would improve the accuracy of μ_s' predictions. Our findings confirm this hypothesis, although the improvements in accuracy are not obvious in all results. When all samples are considered, the implementation of the combined approach was seen to reduce the μ_s' estimation error from 5.6% to 5.5 %, while the error for μ_a increased from 3.2 to 4.0%. When only sam-

ples with $\mu_a > 5$ cm^{-1} were analyzed, μ_s' error improved from 4.6% to 3.7% (an improvement of 20%) while the μ_a error remained constant at 2.2%. Therefore, in general, the implementation of the bifurcated approach produced an improvement in μ_s', possibly at the expense of a slight increase in μ_a error.

The limited success of the bifurcated probe geometry and discrepancy between measured and simulated data at low μ_a values (Figure 6) are likely related to two factors: (1) reflection off the probe face, which was simulated in our model as a perfect absorber and (2) discrepancies between the Henyey-Greenstein phase function used in the current study and the true phase function of the sample. While the probe face is not a perfect absorber, additional simulations performed with our model indicate that even if it were 100% reflective, the increase in detected signal for μ_a = 1 cm^{-1}, μ_s' = 15 cm^{-1} would only be about 15%. Therefore, it is not likely that this is the primary for the discrepancy noted in Figure 6. Prior studies have indicated that for small source-detector separation distances, models based on the Henyey-Greenstein phase function may not produce accurate reflectance predictions due to underestimation of backscattered photons [33,34]. While neither of these prior studies included high μ_a values, Mourant *et al.* provided simulation data for μ_s' = 12.2 cm^{-1} and μ_a = 0–2 cm^{-1} in an adjacent fiber geometry which provides qualitative corroboration of the errors found with our bifurcated probe for $\mu_a < 5$ cm^{-1}. While the Mie phase function employed by Mourant *et al.* produces greater accuracy when simulating the behaviour of microspheres of a single diameter, the benefit of this approach may be reduced in complex biological tissue with a variety of scatterers. One of the only recent studies involving measurements of reflectance with a bifurcated probe showed minimal discrepancy between experimental results and Monte Carlo simulations employing a Henyey-Greenstein phase function [19]. Given these prior results, we believe that a bifurcated approach is valid at least for samples with μ_a values of 5 cm^{-1} or more. However, given the apparent lack of agreement in the literature there exists a need to further elucidate the true effect of phase function on reflectance measurements and in highly attenuating turbid media. Therefore, we intend perform a future study to thoroughly characterize the influence of phase function in highly attenuating samples and thus generate more definitive answers regarding the conditions (e.g., optical properties,

probe geometries, scatterer sizes) for which Henyey-Greenstein and Mie phase functions are valid. Such research will further facilitate the simulation and development of reflectance systems that employ both single- and multi-fiber probes.

Conclusion
This study represents a significant step towards the accomplishment of our long-term goal of performing *in vivo* measurements of tissue optical properties at UVA-VIS wavelengths. Revisions in instrumentation and procedures have improved our system's ability to measure optical properties in turbid media. A rigorous experimental evaluation of this system indicated decreases in average error of 74% and 65% for μ_a and μ_s', respectively, in comparison with our prior study. Given that a mean optical property measurement error of less than 5% has been achieved, our approach has the potential to provide scientifically useful *in vivo* data. The inclusion of reflectance data from the illumination site produced a decrease of 24% in average error for predicting μ_s', yet the validity of this approach for samples with μ_a values of about 5 cm^{-1} or less is questionable and will require further research.

Disclaimer
The opinions and conclusions stated in this paper are those of the authors and do not represent the official position of the U.S. Food and Drug Administration. The mention of commercial products, their sources, or their use in connection with material reported herein is not to be construed as either an actual or implied endorsement of such products by the U.S. Food and Drug Administration.

Authors' contributions
DS calibrated the system, performed measurements of the phantoms, processed the reflectance data, and drafted the manuscript. AA assisted in modifying the experimental system and performing measurements as well as interpretation of the results. LSM designed, constructed and characterized the tissue phantoms. TJP conceived of and designed the study, constructed part of the system, developed the neural network model and helped to draft the manuscript. All authors read and approved the final manuscript.

References
1. Arakawa K, Isoda K, Ito T, Nakajima K, Shibuya T, Ohsuzu F: **Fluorescence analysis of biochemical constituents identifies atherosclerotic plaque with a thin fibrous cap.** *Arterioscler Thromb Vasc Biol* 2002, **22:**1002-1007.
2. Lin WC, Toms SA, Johnson M, Jansen ED, Mahadevan-Jansen A: ***In vivo* brain tumor demarcation using optical spectroscopy.** *Photochem Photobiol* 2001, **73:**396-402.

3.   Ramanujam N: **Fluorescence spectroscopy of neoplastic and non-neoplastic tissues.** *Neoplasia* 2000, **2:**89-117.
4.   Muller MG, Georgakoudi I, Zhang Q, Wu J, Feld MS: **Intrisic fluorescence spectroscopy in turbid media: disentangling effects of scattering and absorption.** *Appl Opt* 2001, **40:**4633-4646.
5.   Skala MC, Palmer GM, Zhu C, Liu Q, Vrotsos KM, Marshek-Stone CL, Gendron-Fitzpatrick A, Ramanujam N: **Investigation of fiber-optic probe designs for optical spectroscopic diagnosis of epithelial pre-cancers.** *Lasers Surg Med* 2004, **34:**25-38.
6.   Pfefer TJ, Agrawal A, Drezek RA: **Oblique-incidence illumination and collection for depth-selective fluorescence spectroscopy.** *J Biomed Opt* 2005, **10:**44016.
7.   Cheong WF: **Appendix to Chapter 8: Summary of optical properties.** In *Optical-Thermal Response of Laser-irradiated Tissue* Edited by: Welch AJ, van Gemert MCJ. Plenum Press, New York; 1995:275-303.
8.   Patterson MS, Chance B, Wilson BC: **Time resolved reflectance and transmittance for the noninvasive measurements of optical properties.** *Appl Opt* 1989, **28:**2331-2336.
9.   Fantini S, Francechini-Fantini MA, Maier JS, Walker SA, Barbieri B, Gratton E: **Frequency-domain multichannel optical detector for noninvasive tissue spectroscopy and oximetry.** *Opt Eng* 1995, **34:**32-42.
10. Kienle A, Lilge L, Patterson M, Hibst R, Steiner R, Wilson B: **Spatially resolved absolute diffuse reflectance measurements for non-invasive determination of the optical scattering and absorption coefficients of biological tissue.** *Appl Opt* 1996, **35:**2304-2314.
11. Dam JS, Pedersen CB, Dalgaard T, Fabricius PE, Aruna P, Andersson-Engels S: **Fiber-optic probe for noninvasive real-time determination of tissue optical properties at multiple wavelengths.** *Appl Opt* 2001, **40:**1155-1164.
12. Pham T, Bevilacqua F, Spott T, Dam J, Tromberg B: **Quantifying the absorption and reduced scattering coefficients of tissuelike turbid media over a broad spectral range with noncontact Fourier-transform hyperspectral imaging.** *Appl Opt* 2000, **39:**6487-6497.
13. Farrell TJ, Patterson MS: **A diffusion theory model of spatially resolved, steady-state diffuse reflectance for the noninvasive determination of tissue optical properties *in vivo.*** *Med Phys* 1992, **19:**879-888.
14. Nichols M, Hull E, Foster T: **Design and testing of a white-light, steady-state diffuse reflectance spectrometer for determination of optical properties of highly scattering systems.** *Appl Opt* 1997, **36:**93-104.
15. Mourant JR, Bigio IJ, Jack DA, Johnson TM: **Measuring absorption coefficients in small volumes of highly scattering media: source-detector separations for which path lengths do not depend on scattering properties.** *Appl Opt* 1997, **36:**5655-5661.
16. Farrell TJ, Wilson BC, Patterson MS: **The use of a neural network to determine tissue optical properties from spatially resolved diffuse reflectance measurements.** *Phys Med Biol* 1992, **37:**2281-2286.
17. Doornbos RMP, Lang R, Aalders MC, Cross FW, Sterenbourg HJC: **The determination of *in vivo* human tissue optical properties and absolute chromophore concentrations using spatially resolved steady-state diffuse reflectance spectroscopy.** *Phys Med Biol* 1999, **44:**967-981.
18. Bays R, Wagnieres G, Robert D, Mizeret J, Braichotte D, van den Bergh H: **Clinical measurements of tissue optical properties in the esophagus.** *Proc. SPIE: Optical Biopsy and Fluorescence Spectroscopy and Imaging* 1995, **2324:**39-45.
19. Moffitt TP, Prahl SA: **Sized-fiber reflectometry for measuring local optical properties.** *IEEE J Sel Top Quantum Electron* 2001, **7:**952-958.
20. Bruulsema JT, Hayward JE, Farrell TJ, Patterson MS, Heinemann L, Berger M, Koschinsky T, Sandahl-Christiansen J, Orskov H, Essenpreis M, Schmelzeisen-Redeker G, Bocker D: **Correlation between blood glucose concentration in diabetics and noninvasively measured tissue optical scattering coefficient.** *Opt Lett* 1997, **22:**190-192.
21. Dam JS, Anderson PE, Dalgaard T, Fabricius PE: **Determination of tissue optical properties from diffuse reflectance profiles by multivariate calibration.** *Appl Opt* 1998, **37:**772-778.
22. Berger AJ, Venugopalan V, Durkin AJ, Pham T, Tromberg BJ: **Chemometric analysis of frequency-domain photon migration data: Quantitative measurements of optical properties and chromophore concentrations in multicomponent turbid media.** *Appl Opt* 2000, **39:**1659-67.
23. Pfefer TJ, Matchette LS, Bennett CL, Gall JA, Wike JN, Durkin AJ, Ediger MN: **Reflectance-based determination of optical properties in highly attenuating tissue.** *J Biomed Opt* 2003, **8:**206-215.
24. Weersink R, Hayward J, Diamond K, Patterson M: **Accuracy of non-invasive *in vivo* measurements of photosensitizer uptake based on a diffusion model of reflectance spectroscopy.** *Photochem Photobiol* 1997, **66:**326-335.
25. Pfefer TJ, Matchette LS, Ross AM, Ediger MN: **Selective detection of fluorophore layers in turbid media: the role of fiberoptic probe design.** *Opt Lett* 2003, **28:**120-122.
26. Prahl SA, van Gemert MJC, Welch AJ: **Determining the optical properties of turbid media by using the adding-doubling method.** *Appl Opt* 1993, **32:**559-568.
27. Durkin AJ, Jaikumar S, Richards-Kortum R: **Optically dilute, absorbing, and turbid phantoms for fluorescence spectroscopy of homogeneous and inhomogeneous samples.** *Appl Opt* 1993, **47:**2114-2121.
28. Graaff R, Aarnoudse JG, de Mul FFM, Jentink HW: **Similarity relations for anisotropic scattering in absorbing media.** *Opt Eng* 1993, **32:**244-252.
29. Madsen SJ, Patterson MS, Wilson BC: **The use of India ink as an optical absorber in tissue-simulating phantoms.** *Phys Med Biol* 1992, **37:**985-993.
30. Jacques SL, Wang L: **Chapter 4: Monte Carlo modeling of light transport in tissues.** In *Optical-Thermal Response of Laser-irradiated Tissue* Edited by: Welch AJ, van Gemert MCJ. Plenum Press, New York; 1995:275-303.
31. Liu Q, Zhu C, Ramanujam N: **Experimental validation of Monte Carlo modeling of fluorescence in tissues in the UV-Visible spectrum.** *J Biomed Opt* 2003, **8:**223-236.
32. Theuler P, Charvet I, Bevilacqua F, Ghislain M St, Ory G, Marquet P, Meda P, Vermeulen B, Depeursinge C: ***In vivo* endoscopic tissue diagnostics based on spectroscopic absorption, scattering, and phase function properties.** *J Biomed Opt* 2003, **8:**495-503.
33. Mourant JR, Boyer J, Hielscher AH, Bigio IJ: **Influence of the scattering phase function on light transport measurements in turbid media performed with small source-detector separations.** *Optics Lett* 1996, **21:**546-548.
34. Bevilacqua F, Depeursinge C: **Monte Carlo study of diffuse reflectance at source-detector separations close to one transport mean free path.** *J Opt Soc Am A* 1999, **16:**2935-2945.